Article

In Situ-Grown Al$_2$O$_3$ Nanoflowers and Hydrophobic Modification Enable Superhydrophobic SiC Ceramic Membranes for Membrane Distillation

Yuqi Song [1], Kai Miao [1], Jinxin Liu [1], Yutang Kang [1], Dong Zou [1,*] and Zhaoxiang Zhong [1,2,*]

[1] School of Environmental Science and Engineering, Nanjing Tech University, Nanjing 211816, China; syq2023@njtech.edu.cn (Y.S.); mk@njtech.edu.cn (K.M.); jinxinliu@njtech.edu.cn (J.L.); kangyt@njtech.edu.cn (Y.K.)

[2] National Engineering Research Center for Special Separation Membrane, College of Chemical Engineering, Nanjing Tech University, Nanjing 211816, China

* Correspondence: zoudong@njtech.edu.cn (D.Z.); zhongzx@njtech.edu.cn (Z.Z.)

Abstract: Membrane distillation (MD) is considered a promising technology for desalination. In the MD process, membrane pores are easily contaminated and wetted, which will degrade the permeate flux and salt rejection of the membrane. In this work, SiC ceramic membranes were used as the supports, and an Al$_2$O$_3$ micro-nano structure was constructed on its surface. The surface energy of Al$_2$O$_3$@SiC micro-nano composite membranes was reduced by organosilane grafting modification. The effective deposition of Al$_2$O$_3$ nanoflowers on the membrane surface increased membrane roughness and enhanced the anti-fouling and anti-wetting properties of the membranes. Simultaneously, the presence of nanoflowers also regulated the pore structures and thus decreased the membrane pore size. In addition, the effects of Al$_2$(SO$_4$)$_3$ concentration and sintering temperature on the surface morphology and performance of the membranes were investigated in detail. It was demonstrated that the water contact angle of the resulting membrane was 152.4°, which was higher than that of the pristine membrane (138.8°). In the treatment of saline water containing 35 g/L of NaCl, the permeate flux was about 11.1 kg·m^{-2}·h^{-1} and the salt rejection was above 99.9%. Note that the pristine ceramic membrane cannot be employed for MD due to its larger membrane pore size. This work provides a new method for preparing superhydrophobic ceramic membranes for MD.

Keywords: ceramic membrane; Al$_2$O$_3$ nanoflowers; superhydrophobic surface; vacuum membrane distillation

1. Introduction

The problem of water scarcity is becoming severer due to industrial pollution and climate change. Desalination technology has the potential to alleviate the shortage of freshwater resources. Membrane distillation (MD) technology, as an emerging desalination technique, is receiving increasing attention because of its high separation efficiency and mild operating conditions [1–3]. MD technology is a separation technique that uses hydrophobic porous membranes to separate saline water. These membranes have a microporous structure. In the MD process, one side of the membrane is the feed side that directly contacts with the feed solution, while the other side is the permeate side. Under the action of vapor pressure difference, the membrane can selectively allow water vapor to pass through and block the passage of saline water, thereby realizing the separation of water and salt [4–7]. Therefore, the salt rejection can theoretically reach 100%.

The commonly used membranes are generally polymer membranes, such as polyvinylidene fluoride (PVDF), polypropylene (PP), polyethylene (PE) and polytetrafluoroethylene (PTFE) membranes [8–10]. However, polymer membranes cannot be employed under critical conditions for a long time due to their poor chemical and mechanical properties.

In contrast, ceramic membranes have better thermal stability and mechanical stability, and can also be employed under harsh conditions [11–13]. As a result, ceramic membranes have gradually attracted attention in MD applications [14]. However, ceramic membranes are hydrophilic due to the existence of a large number of hydroxyl groups on the surface, so it is necessary to modify the surface of ceramic membranes to make them hydrophobic [15]. The commonly used method at present is to directly modify the membrane hydrophobicity using fluorosilane. However, membranes modified directly through traditional methods often exhibit poor hydrophobicity and are prone to being wetted. Wei et al. used a conventional hydrophobic modification method to modify the ceramic membrane and found that asymmetric porous cordierite ceramic membranes directly modified by 1H,1H,2H,2H-perfluorodecyl -triethoxysilane (PFDTS) experienced severe wetting after a 6 h MD process [16]. How to improve the stability and hydrophobicity of ceramic membranes in the MD process is challenging.

As is well known to all, surface roughness plays a crucial role in the hydrophobicity of membranes [17]. Based on the Cassie theory, rough micro-nano structures can trap more air, forming an air layer on the membrane surface, thereby reducing the contact area between the liquid and the membrane surface, making it easy for the liquid to slip off the membrane surface [18–20]. Currently, enhancing membrane roughness is mainly achieved by depositing inorganic nano-sized particles (such as ZnO, TiO_2, SiO_2, CuO, etc.) on the membrane surface to construct a reentrant structure [21–23]. For example, Chen et al. [24] deposited ZnO nanorods and nanoparticles on the surface of Al_2O_3 hollow fiber membranes using the chemical bath deposition method, increasing the roughness from 93.41 nm to 186.34 nm, enhancing the wetting resistance of the membrane. Mohd et al. [25] synthesized TiO_2 nanoflowers and nanorods on mullite hollow fiber membranes via the hydrothermal method, increasing the roughness from 51.4 nm to 136.8 nm. The prepared membrane obtained a satisfactory water contact angle of 162°, demonstrating excellent hydrophobic properties. However, there is currently limited research on the application of the in situ growth of Al_2O_3 nanoflowers on ceramic membranes via the hydrothermal method for MD.

In this work, the hydrothermal method was utilized successfully to obtain the in situ growth of Al_2O_3 nanoflowers with different scales on SiC membranes. Additionally, the membranes were modified using organosilane to lower the surface energy to fabricate superhydrophobic Al_2O_3@SiC composite ceramic membranes. These nanoflowers cannot only increase the membrane roughness but also regulate the pore structures of the membrane (see Figure 1). The concentration of the Al^{3+} precursor and the sintering temperature were investigated in detail for their impact on the microstructure of the resulting membrane. The prepared composite ceramic membranes were also characterized using SEM, XRD, XPS, etc. Moreover, the vacuum membrane distillation (VMD) performance of the prepared membranes was investigated.
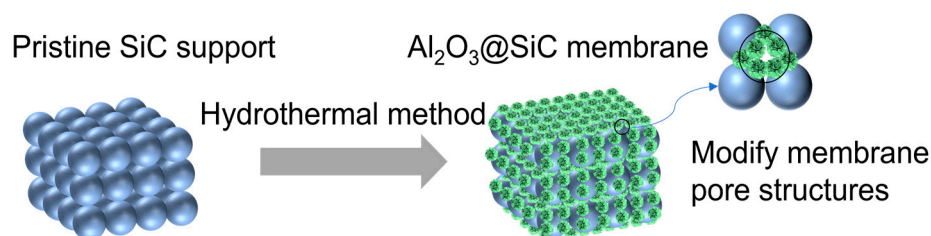

Figure 1. Scheme of the in situ growth of Al_2O_3 nanoflowers.

2. Materials and Methods

2.1. Materials

Aluminum sulfate ($Al_2(SO_4)_3$, AR) was purchased from Meryer Chemical Technology Co., Ltd. (Shanghai, China). Urea ($CO(NH_2)_2$, 99%); 1H,1H,2H,2H-perfluorodecyl -triethoxysilane (PFDTS, 98%) and sodium chloride (NaCl, 99.5%) were purchased from Shanghai Aladdin Biochemical Technology Co., Ltd. (Shanghai, China). SiC supports

were fabricated from SiC powders with a particle size of 5 microns. Deionized (DI) water produced by a pure water machine of Nanjing Yuheng Instrument and Equipment Co., Ltd (Nanjing, China) was used in all experiments.

2.2. Preparation of Superhydrophobic SiC Ceramic Membranes

2.2.1. Preparation of SiC Supports

SiC supports were fabricated from SiC powders with a particle size of 5 microns. Five-micron SiC powders were used as the supporting aggregates, and an 8 wt% PVA solution was used as binders. After thorough mixing, the green body (unsintered SiC support) was obtained by a dry pressing process with the pressing time of 40 s and holding pressure of 10 MPa. Subsequently, SiC supports were obtained through sintering at 1300 °C. SiC supports are circular in shape, and they are discs (the thickness of the disc is 2.1 mm and the diameter is 31 mm).

2.2.2. In Situ Growth of Al_2O_3 Nanoflowers

The growth of Al_2O_3 nanoflowers on the surface of SiC membranes was first carried out using the hydrothermal method, followed by sintering. The pristine SiC supports were washed by ethanol for 5 min and dried at 60 °C for 30 min. The precursor solution was prepared by adding $Al_2(SO_4)_3$ (with concentrations of 0.0875 M, 0.175 M, 0.2625 M) and urea (with the concentration of 2.22 M) into 30 mL of deionized (DI) water. Then, the solution was stirred thoroughly to obtain a clear and transparent solution. The SiC supports were vertically placed into the Teflon lining and then the precursor solution was poured into it. Subsequently, the SiC supports were reacted at 160 °C for 8 h. Then, the membranes were washed thoroughly by DI water. Subsequently, membranes were dried under a vacuum for 24 h. After that, membranes were sintered at different temperatures (600 °C, 900 °C or 1200 °C) for 12 h.

2.2.3. Hydrophobic Modification

Firstly, a 2 vol% C8 solution was prepared by adding 1 mL of 1H,1H,2H,2H-Perfluorodecyl-triethoxysilane into 49 mL of ethanol. Secondly, the fluorination solution was sonicated by a sonicator for 5 min to ensure uniform mixing. Then, the prepared SiC ceramic membranes were immersed in the fluorination solution at 60 °C for 48 h. Subsequently, membranes underwent condensation polymerization at 120 °C for 3 h. The specific sample codes with different reaction processes are detailed in Table 1.

Table 1. Sample codes with different reaction processes.

Sample Codes	$Al_2(SO_4)_3$ Concentration (M)	Sintering Temperature (°C)	Fluorinated/ Unfluorinated
SiC-C_1	0.0875	600	Unfluorinated
SiC-C_2/SiC-T_1	0.175	600	Unfluorinated
SiC-C_3	0.2625	600	Unfluorinated
SiC-T_2	0.175	900	Unfluorinated
SiC-T_3	0.175	1200	Unfluorinated
SiC-C_1-f	0.0875	600	Fluorinated
SiC-C_2-f/SiC-T_1-f	0.175	600	Fluorinated
SiC-C_3-f	0.2625	600	Fluorinated
SiC-T_2-f	0.175	900	Fluorinated
SiC-T_3-f	0.175	1200	Fluorinated

2.3. Characterization

Membrane surface morphology was examined by desktop scanning electron microscopy (Hitachi TM3000, Hitachi, Japan) and field-emission SEM (Hitachi S-4800, Hitachi, Japan). Pore size distribution of the membranes was measured using a capillary flow porometer (PMI ipore 1500, PMI, Ithaca, NY, USA). The water contact angle was measured

by Dataphysios OCA25 (OCA 25, Dataphysios, Filderstadt, Germany). Surface roughness was observed by a surface profiler (PARK XE-100, Park Systems, Santa Clara, CA, USA). X-ray diffraction analysis was conducted by an X-ray diffractometer (RIGAKU MiniFlex600, Rigaku, Tokyo, Japan). The surface elements of the membranes were analyzed by X-ray Photoelectron Spectroscopy (XPS, Thermo Fisher Scientific Escalab, Waltham, MA, USA).

2.4. Vacuum Distillation Experiment

VMD tests were carried out using a laboratory-made setup. The membrane distillation setup is shown in Figure 2. In the MD application, the feed solution was heated in a water bath at 70 °C and then flowed under the action of a peristaltic pump. The flow rate was 200 mL/min. The vacuum degree was −0.090 MPa. When the feed liquid contacted the membrane surface, generated water vapor permeated through the membrane and condensed into liquid water. After a fixed period of time, the weight of the liquid in the flask was measured, along with its conductivity
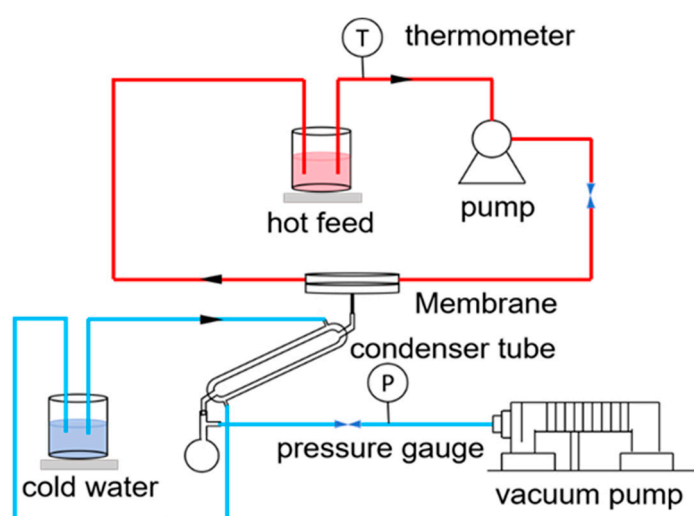

Figure 2. Schematic diagram of the VMD apparatus.

Equation (1) can be used to calculate the permeate flux J (kg·m^{-2}·h^{-1}) of the membranes:

$$J = \frac{m}{A \cdot \Delta t} \tag{1}$$

where m represents the mass of the permeate water (kg), A represents the effective area of the membranes (m^2) and Δt is the interval time (h).

Equation (2) can be used to calculate the salt rejection R (%) of the membranes:

$$R = \frac{C_1 - C_2}{C_1} \times 100\% \tag{2}$$

where R represents the salt rejection (%), C_1 represents the conductivity of the feed solution (uS/cm) and C_2 represents the conductivity of the resulting water.

3. Results and Discussion

3.1. Characterization of Pristine SiC Support

Figure 3a displays the surface morphology of the pristine SiC support, which consisted of irregular particles. The membrane surface was smooth without any obvious defects. Figure 3b shows the pore size distribution of the SiC support. It can be seen that the average pore size was about 1.56 μm. Note that the pore size of the membrane was large (>1 μm) and the feed solution can easily wet the membrane [26]. Thus, the pristine SiC support was not suitable for MD application directly.

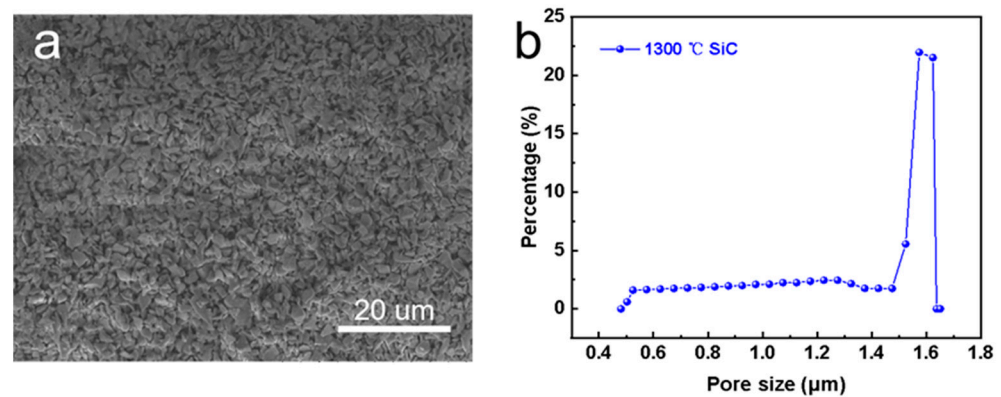**Figure 3.** Characterization of pristine SiC support. (**a**) Surface morphology, and (**b**) pore size distribution.

3.2. Effects of $Al_2(SO_4)_3$ Concentration

Based on the above discussion, it is meaningful to decrease the pore size of the SiC support. In situ growth of inorganic nanoflowers can regulate the pore size and surface roughness simultaneously. Herein, Al_2O_3 nanoflowers were proposed to decorate the membrane structures. The concentration of $Al_2(SO_4)_3$ in the precursor solution significantly influenced the in situ growth of Al_2O_3 nanoflowers. When the sintering temperature was 600 °C, the surface morphologies of membranes prepared using varying $Al_2(SO_4)_3$ concentrations are illustrated in Figure 4. At an $Al_2(SO_4)_3$ concentration of 0.0875 M, the formation of a flower-like structure was not prominent. Instead, leaf-like structures were observed, which were inadequately distributed on the membrane surface and the surface remained relatively smooth. Additionally, there were still some macropores to be observed on the membrane surface. When the concentration of $Al_2(SO_4)_3$ was 0.175 M, nanoflowers were evenly distributed on the membrane surface. When the $Al_2(SO_4)_3$ concentration was increased to 0.2625 M, more nanoflowers appeared on the membrane surface, resulting in a hierarchical structure. As the $Al_2(SO_4)_3$ concentration increased, there was a gradual increase in both the number and size of nanoflowers. This could be attributed to the low concentration of $Al_2(SO_4)_3$, which failed to provide sufficient Al^{3+} to react effectively with urea.
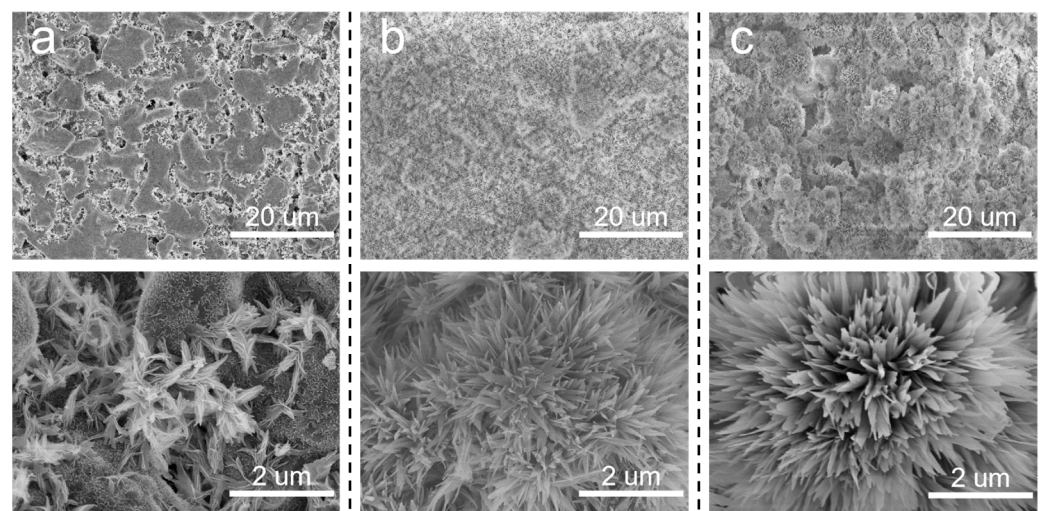

Figure 4. Surface morphologies of Al_2O_3@SiC composite membranes fabricated with different $Al_2(SO_4)_3$ concentrations. (**a**) 0.0875 M, (**b**) 0.175 M and (**c**) 0.2625 M.

To further determine the concentration of $Al_2(SO_4)_3$, the pore size distributions of the membranes with different $Al_2(SO_4)_3$ concentrations were investigated (see Figure 5a). The mean pore sizes of SiC-C_1, SiC$_2$ and SiC-C_3 were around 1.37 um, 0.51 um and

0.37 um, respectively. The grown nanoflowers modified the membrane pore structures and thus decreased the membrane pore size, which was consistent with the SEM image in Figure 4. The surface roughness plays an important role in the hydrophobic properties of the membranes. The surface roughnesses of the prepared membranes were characterized by the surface profiler (See Figure 5b–e). The surface roughness of the pristine support was only 1.321 μm. After the in situ growth of Al_2O_3 nanoflowers on the membrane surface, the surface roughness of the membrane initially increased and then remained stable. The roughness of the SiC-C_1 was only 1.443 μm. When the $Al_2(SO_4)_3$ concentration was 0.175 M, the roughness increased to 2.056 um. When the concentration of $Al_2(SO_4)_3$ further increased to 0.2625 M, the membrane roughness did not have an obvious change, with a roughness of 2.012 μm. The membrane roughness increased after the in situ growth of Al_2O_3 nanoflowers compared to the pristine supports. A rough membrane surface can store more air, leading to the presence of air pockets between the membrane surface and the feed liquid, and then reduce the contact area, enhancing the hydrophobic performance of the membranes. In summary, the most suitable concentration of $Al_2(SO_4)_3$ was 0.175 M.

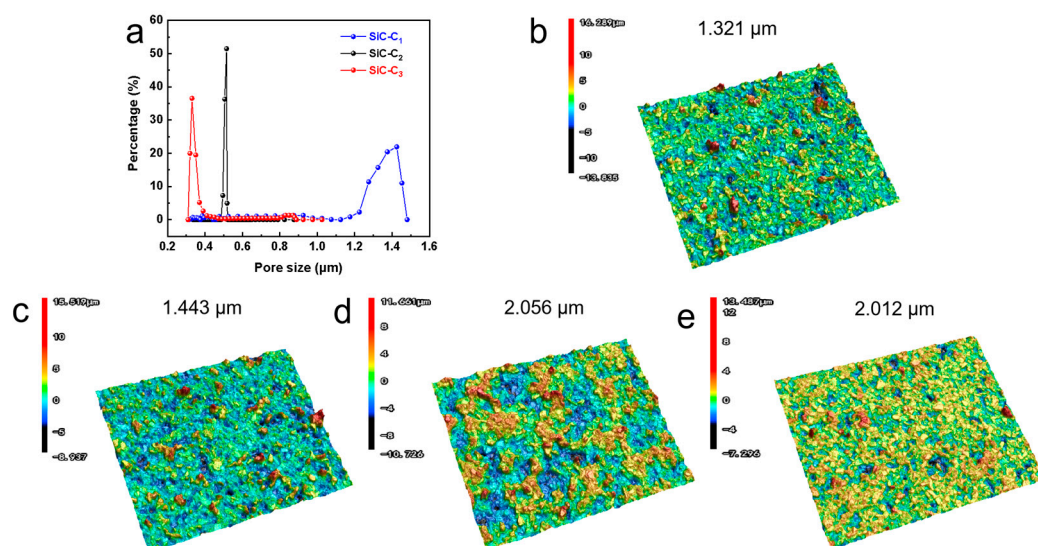**Figure 5.** (**a**) Pore size distribution. Three-dimensional surface morphology of (**b**) pristine, (**c**) SiC-C_1, (**d**) SiC-C_2 and (**e**) SiC-C_3.

3.3. Effects of Sintering Temperature

In addition to the concentration of the precursor solution, the effects of the sintering temperature after the hydrothermal treatment on the prepared membranes were also investigated. It can be observed from Figure 6 that flower-like nanostructures were formed on the membrane surfaces at different sintering temperatures. However, as the sintering temperature rose, the number and size of flower-like structures on the membrane surface gradually decreased. SiC-T_1 and SiC-T_2 exhibited a significant presence of nanoflowers on the surface of membranes, while the surface of SiC-T_3 appeared smoother with noticeable block-like structures of SiC particles, and the nanoflowers mainly existed within the pores formed by SiC particles. When the precursor concentrations were the same, the size of the formed nanoflower via the hydrothermal method remained the same. However, as the sintering temperature increased, the resulting crystal structure exhibited a larger apparent density, leading to a reduction in size and number after being sintered at higher temperatures. It can be observed from Figure 7 that the average pore sizes of SiC-T_1, SiC-T_2 and SiC-T_3 were 0.51 um, 0.62 um and 0.71 um, respectively. As the sintering temperature rose, the average pore size of the Al_2O_3@SiC composite ceramic membranes increased continuously, which was also in line with the SEM images. In summary, the most suitable sintering temperature was 900 °C.
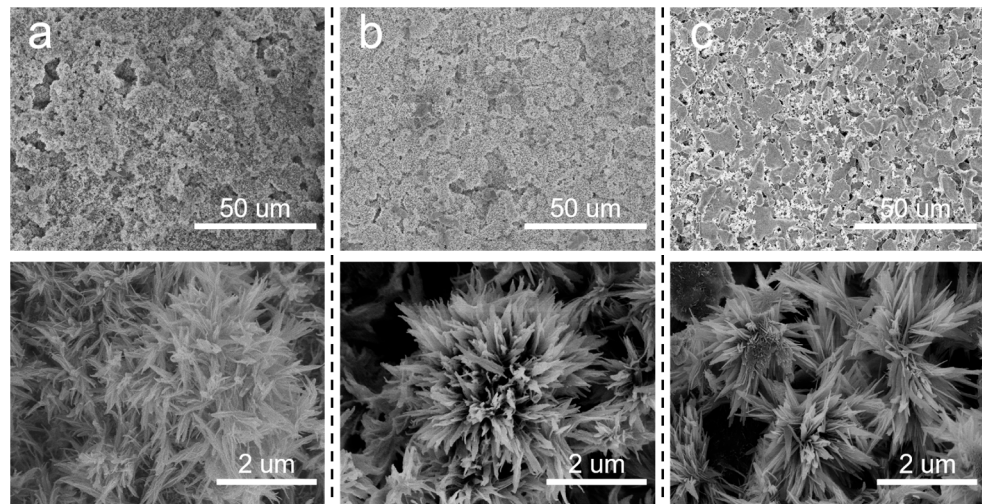
Figure 6. Surface morphology of Al_2O_3@SiC composite membranes fabricated at different sintering temperatures. (**a**) 600 °C, (**b**) 900 °C and (**c**) 1200 °C.

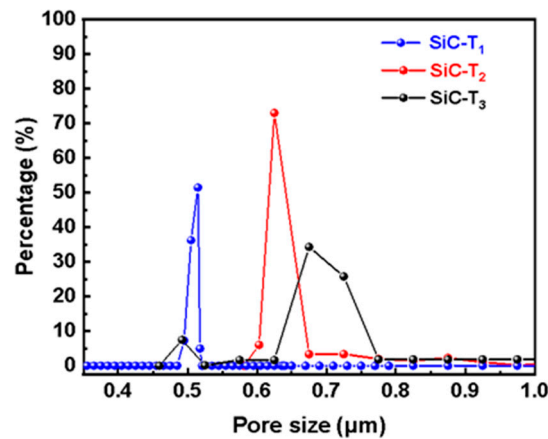**Figure 7.** Pore size distribution of Al_2O_3@SiC composite ceramic membranes fabricated at different sintering temperatures.

3.4. XRD Analysis of Al_2O_3 Nanoflowers Synthesized via Hydrothermal Method

The XRD patterns in Figure 8a show the unsintered Al_2O_3 nanoflower powders obtained from the hydrothermal reaction of urea and varying concentrations of $Al_2(SO_4)_3$ at 160 °C for 8 h. It can be seen that the XRD patterns of the obtained powders are similar at different $Al_2(SO_4)_3$ concentrations with diffraction characteristic peaks appearing at 14.48°, 28.18°, 38.34° and 48.93°, respectively. Compared with the diffraction card of boehmite (JCPDS 21-1307), it was found that they corresponded to the (020), (120), (031) and (200) crystal planes of the boehmite phase. This was attributed to the hydrolysis of urea in the autoclave at 160 °C that generated OH^- and NH_4^+. Subsequently, Al^{3+} reacted with OH^- to form $Al(OH)_3$ colloidal. The $Al(OH)_3$ colloid dissolved and recrystallized in the hydrothermal solution, ultimately forming boehmite microcrystals [27]. Note that the powders also contained byproducts such as ammonium sulfate and ammonium bicarbonate.
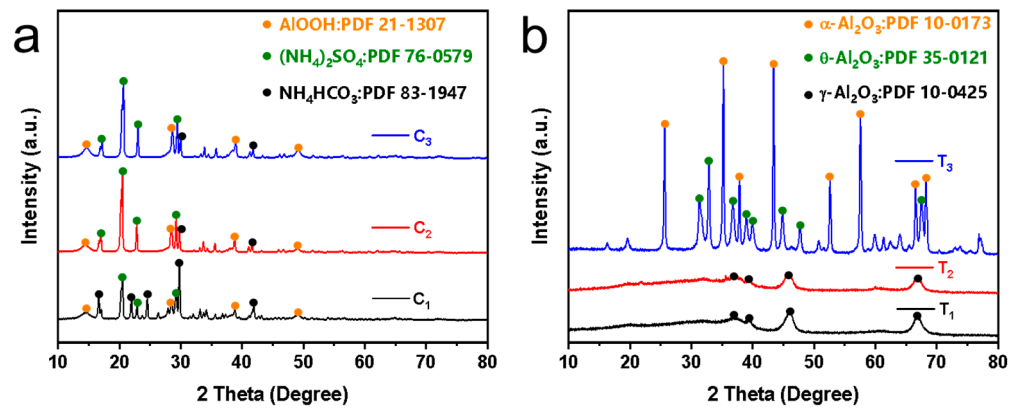
Figure 8. XRD patterns: (**a**) Unsintered powders synthesized by different $Al_2(SO_4)_3$ concentrations, and (**b**) powders sintered at different temperatures. Note that C_1, C_2 and C_3 represent $Al_2(SO_4)_3$ concentrations of 0.0875 M, 0.175 M and 0.2625 M, respectively. T_1, T_2 and T_3 represent powders sintered at 600 °C, 900 °C and 1200 °C, respectively.

Figure 8b shows the XRD patterns of the powders sintered at different temperatures. It was observed that the XRD patterns of powders sintered at 600 °C and 900 °C were similar with diffraction characteristic peaks appearing at 37.60°, 39.49°, 45.86° and 67.03°, respectively. Compared with the diffraction standard card of γ-Al_2O_3 (JCPDS 10-0425), it was found that they corresponded to the (311), (222), (400) and (440) crystal planes of γ-Al_2O_3, respectively. When the powders were sintered at 1200 °C, the XRD pattern corresponded to the diffraction standard cards of θ-Al_2O_3 (JCPDS 35-0121) and α-Al_2O_3 (JCPDS 10-0173). The peaks observed at 31.47°, 32.78°, 36.68°, 38.92°, 39.86°, 44.83°, 47.62° and 67.42° corresponded to the (004), (20-2), (111), (104), (20-4), (21-1), (006) and (215) crystal planes of θ-Al_2O_3 (JCPDS 35-0121). Additionally, the peaks at 25.58°, 35.13°, 37.78°, 43.36°, 57.52°, 66.55°, 68.19° and 76.88° corresponded to the (012), (104), (110), (113), (116), (214) and (300) crystal planes of α-Al_2O_3 (JCPDS 10-0173) [28]. This indicated that the in situ-synthesized nanoflowers sintered at different temperatures were Al_2O_3. When the sintering temperature was 600 °C and 900 °C, γ-Al_2O_3 was formed on the membrane surface, and when the sintering temperature reached 1200 °C, α-Al_2O_3 and θ-Al_2O_3 were formed on the membrane surface.

3.5. Hydrophobic Modification and Membrane Distillation

After investigating the fabrication parameters of the membranes, the Al_2O_3 nanoflower-grown SiC composite membranes were produced successfully under the optimized conditions. Finally, the membranes were hydrophobically modified and characterized. XPS was carried out to analyze the chemical composition of the membrane surface deposited by Al_2O_3 nanoflowers. As shown in Figure 9a, two peaks were observed at 74.38 eV and 531.2 eV in the spectrum of the non-fluorinated membranes, corresponding to Al2p and O1s, respectively. Additionally, a peak was observed at around 689.09 eV in the spectrum of the fluorinated membranes (corresponding to F1s). The O1s spectrum of the non-fluorinated membranes is shown in Figure 9b with a prominent peak at 530.1 eV (assigned to O-Al), indicating the successful deposition of Al_2O_3 on the membrane surface [29]. Figure 9c displays the C1s spectrum of the fluorinated membranes, showing two prominent peaks at 294.78 eV (assigned to CF3) and 292.1 eV (assigned to CF2), indicating successful fluorination [30].
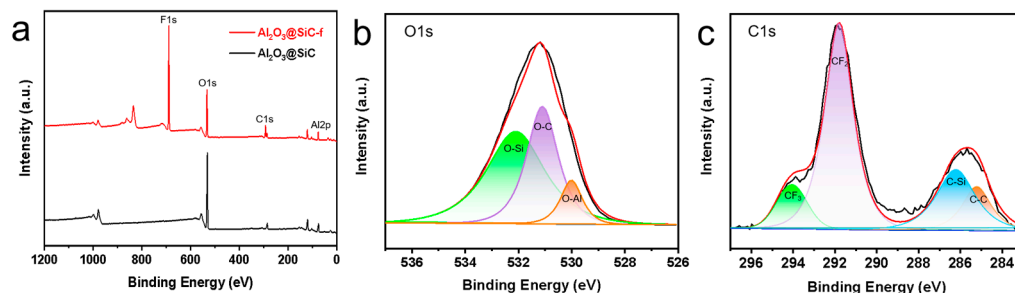
Figure 9. (**a**) XPS spectra of Al$_2$O$_3$@SiC membranes and Al$_2$O$_3$@SiC-f membranes, (**b**) decomposition of O1s in Al$_2$O$_3$@SiC membranes and (**c**) decomposition of C1s in Al$_2$O$_3$@SiC-f membranes.

The SiC-T$_1$-f, SiC-T$_2$-f and SiC-T$_3$-f membranes were selected for MD application. Note that the data reported in Figure 10 were obtained after a 12 h MD process. Due to the in situ growth of numerous micro-nanostructures on the surface, the contact angle of the SiC-T$_1$-f membrane can reach 152.7° (see Table 2), but the initial permeate flux of the SiC-T$_1$-f membrane was exceptionally low when treating saline water containing 35 g/L of NaCl at 70 °C (only 7.41 kg·m^{-2}·h^{-1}) (see Figure 10a). SiC-T$_3$-f's contact angle can reach 150.5° (see Table 2). Because of the presence of some large membrane pores, the feed can directly pass through SiC-T$_3$'s pores, resulting in a lower salt rejection. By contrast, SiC-T$_2$-f was more appropriate for MD. Aside from the appropriate pore size distribution and distribution density of Al$_2$O$_3$ nanoflowers, SiC-T$_2$-f's water contact angle also reached 152.4° (see Table 2). When the feed solution was distilled water, SiC-T$_2$-f's permeate flux was 12.5 kg·m^{-2}·h^{-1}. In the treatment of saline water containing 35 g/L of NaCl at 70 °C, the permeate flux was about 11.1 kg·m^{-2}·h^{-1} and the salt rejection was above 99.9% (see Figure 10b). Table 3 displays the ceramic membrane properties of MD reported in previous works. It is demonstrated that the water flux of the resulting ceramic membranes in this work is satisfactory.
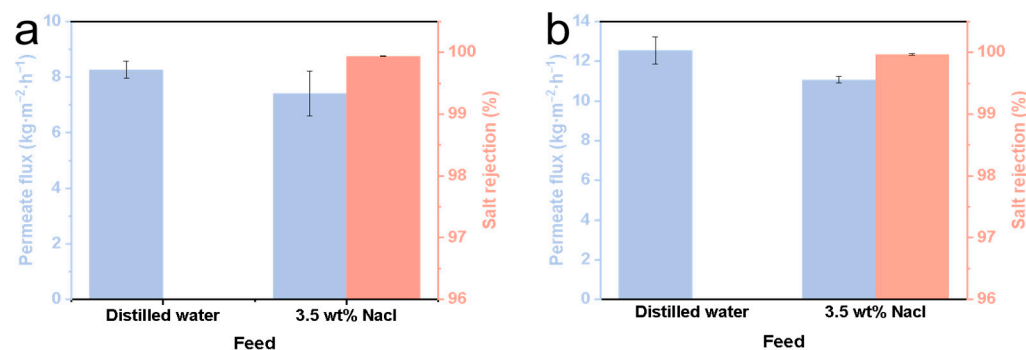

Figure 10. Permeate flux of (**a**) SiC-T$_1$-f and (**b**) SiC-T$_2$-f.

Table 2. Contact angle of the membranes.

Sample Codes	Contact Angle (°)
SiC	138.8
SiC-T$_1$-f	152.7
SiC-T$_2$-f	152.4
SiC-T$_3$-f	150.5

Table 3. Ceramic membrane properties for MD reported in previous works.

Refs.	Membrane Material	Concentration of the NaCl/g L^{-1}	Permeate Flux/kg·m^{-2}·h^{-1}	Salt Rejection/%
[31]	Si_3N_4	20	12	99
[32]	SiC	50	0.13	98
[25]	Mullite	35	4.32	99.99
This work	SiC	35	11.1	99.9

4. Conclusions

In this work, superhydrophobic Al_2O_3@SiC composite ceramic membranes were fabricated successfully. The presence of nanoflowers cannot only regulate the pore structures, but also increase the surface roughness, thus improving hydrophobicity and enhancing resistance to fouling and wetting. The effects of precursor solution concentration and sintering temperature on the morphology and performance of membranes were investigated. An appropriate preparation condition was determined through SEM, pore size distribution and MD performance. Results show that the optimal concentration of $Al_2(SO_4)_3$ was 0.175 M and the optimal sintering temperature was 900 °C. The roughness of the prepared membrane increased from 2.056 μm to 1.321 μm and the water contact angle was about 152.4°. In the treatment of saline water containing 35 g/L of NaCl at 70 °C, the permeate flux was about 11.1 kg·m^{-2}·h^{-1} and the salt rejection was above 99.9%. Currently, there are few reports on the growth of Al_2O_3 nanoflowers on ceramic membranes. This work provides a new approach for preparing superhydrophobic ceramic membranes. However, the long-term stability of this membrane is not satisfactory that should be further investigated in detail by finely-tuning the pore size of the ceramic support and microstructures of the membrane.

Author Contributions: Conceptualization, D.Z.; methodology, Y.S.; software, Y.S. and K.M.; validation, Y.S. and K.M.; formal analysis, Y.S. and K.M.; investigation, Y.S. and K.M.; resources, D.Z.; data curation, Y.S. and K.M.; writing—original draft preparation, Y.S.; writing—review and editing, Y.S., J.L., Y.K., D.Z. and Z.Z.; visualization, Y.S. and D.Z.; supervision, D.Z. and Z.Z.; project administration, D.Z.; funding acquisition, D.Z. All authors have read and agreed to the published version of the manuscript.

Institutional Review Board Statement: Not applicable.

Data Availability Statement: Data are contained within the article.

Conflicts of Interest: The authors declare no conflicts of interest.

References

1. Chiam, C.-K.; Sarbatly, R. Vacuum membrane distillation processes for aqueous solution treatment—A review. *Chem. Eng. Process.* **2013**, *74*, 27–54. [CrossRef]
2. Wang, P.; Chung, T.-S. Recent advances in membrane distillation processes: Membrane development, configuration design and application exploring. *J. Membr. Sci.* **2015**, *474*, 39–56. [CrossRef]
3. Caspar, J.; Xue, G.; Oztekin, A. Performance characteristics on up-scaling vacuum membrane distillation modules. *Desalination* **2024**, *569*, 116994. [CrossRef]
4. Gontarek-Castro, E.; Castro-Muñoz, R.; Lieder, M. New insights of nanomaterials usage toward superhydrophobic membranes for water desalination via membrane distillation: A review. *Crit. Rev. Environ. Sci. Technol.* **2022**, *52*, 2104–2149. [CrossRef]
5. Deshmukh, A.; Boo, C.; Karanikola, V.; Lin, S.; Straub, A.P.; Tong, T.; Warsinger, D.M.; Elimelech, M. Membrane distillation at the water-energy nexus: Limits, opportunities, and challenges. *Energy Environ. Sci.* **2018**, *11*, 1177–1196. [CrossRef]

6. Venzke, C.; Rizzana, D.; Giacobbo, A.; Rodrigues, M.; He, T.; Bernardes, A. Membrane distillation treating a real petrochemical reverse osmosis concentrate: Influence of membrane characteristics on the process performance. *J. Water Process. Eng.* **2021**, *39*, 101722. [CrossRef]

7. Lin, J.; Du, J.; Xie, S.; Yu, F.; Fang, S.; Yan, Z.; Lin, X.; Zou, D.; Xie, M.; Ye, W. Durable superhydrophobic polyvinylidene fluoride membranes via facile spray-coating for effective membrane distillation. *Desalination* **2022**, *538*, 115925. [CrossRef]

8. Lu, K.-J.; Zuo, J.; Chung, T.-S. Novel PVDF membranes comprising n-butylamine functionalized graphene oxide for direct contact membrane distillation. *J. Membr. Sci.* **2017**, *539*, 34–42. [CrossRef]

9. Gryta, M. Influence of polypropylene membrane surface porosity on the performance of membrane distillation process. *J. Membr. Sci.* **2007**, *287*, 67–78. [CrossRef]

10. Zuo, J.; Bonyadi, S.; Chung, T.-S. Exploring the potential of commercial polyethylene membranes for desalination by membrane distillation. *J. Membr. Sci.* **2016**, *497*, 239–247. [CrossRef]

11. Fung, Y.-L.E.; Wang, H. Nickel aluminate spinel reinforced ceramic hollow fibre membrane. *J. Membr. Sci.* **2014**, *450*, 418–424. [CrossRef]

12. Zhang, J.-W.; Fang, H.; Wang, J.-W.; Hao, L.-Y.; Xu, X.; Chen, C.-S. Preparation and characterization of silicon nitride hollow fiber membranes for seawater desalination. *J. Membr. Sci.* **2014**, *450*, 197–206. [CrossRef]

13. Hubadillah, S.K.; Othman, M.H.D.; Kadir, S.H.S.A.; Jamalludin, M.R.; Harun, Z.; Abd Aziz, M.H.; Rahman, M.A.; Jaafar, J.; Nomura, M.; Honda, S. Removal of As (III) and As (V) from water using green, silica-based ceramic hollow fibre membranes via direct contact membrane distillation. *RSC Adv.* **2019**, *9*, 3367–3376. [CrossRef]

14. Schnittger, J.; Mccutcheon, J.R.; Hoyer, T.; Weyd, M.; Voigt, I.; Lerch, A. Modified ceramic membranes for the treatment of highly saline mixtures utilized in vacuum membrane distillation. *Desalination* **2023**, *567*, 116943. [CrossRef]

15. Wei, J.; Nian, P.; Wang, Y.; Wang, X.; Wang, Y.; Xu, N.; Wei, Y. Preparation of superhydrophobic-superoleophilic ZnO nanoflower@ SiC composite ceramic membranes for water-in-oil emulsion separation. *Sep. Purif. Technol.* **2022**, *292*, 121002. [CrossRef]

16. Teng, H.-D.; Wei, Q.; Wang, Y.-L.; Cui, S.-P.; Li, Q.-Y.; Nie, Z.-R. Asymmetric porous cordierite ceramic membranes prepared by phase inversion tape casting and their desalination performance. *Ceram. Int.* **2020**, *46*, 23677–23685. [CrossRef]

17. Cao, H.; Mao, Y.; Wang, W.; Jin, Y.; Gao, Y.; Zhang, M.; Zhao, X.; Sun, J.; Song, Z. ZIF-8 based dual scale superhydrophobic membrane for membrane distillation. *Desalination* **2023**, *550*, 116373. [CrossRef]

18. Erbil, H.Y.; Cansoy, C.E. Range of applicability of the Wenzel and Cassie–Baxter equations for superhydrophobic surfaces. *Langmuir* **2009**, *25*, 14135–14145. [CrossRef]

19. Wang, R.; Zhang, H.; Zhu, L.; Chen, L.; Ma, W.; Jiang, L.; Zhu, Y.; Wu, B.; Zhang, W. One-step spraying preparation of omniphobic membrane with anti-wetting behavior for membrane distillation. *Desalination* **2023**, *563*, 116719. [CrossRef]

20. Samadi, A.; Ni, T.; Fontananova, E.; Tang, G.; Shon, H.; Zhao, S. Engineering antiwetting hydrophobic surfaces for membrane distillation: A review. *Desalination* **2023**, *563*, 116722. [CrossRef]

21. Sun, B.; Wu, M.; Zhen, H.; Jia, Y.; Li, P.; Yuan, Z.; Li, X.; He, G.; Jiang, X. Tailored PVDF membrane with coordinated interfacial nano/micro-structure for enhanced membrane distillation. *Desalination* **2024**, *573*, 117177. [CrossRef]

22. Omar, N.M.A.; Othman, M.H.D.; Tai, Z.S.; Amhamed, A.O.A.; Yuliwati, E.; Puteh, M.H.; Kurniawan, T.A.; Rahman, M.A.; Jaafar, J.; Ismail, A.F. Robust omniphobic ceramic hollow fibre membrane with leaf-like copper oxide hierarchical structure by membrane distillation. *Desalination* **2023**, *564*, 116816. [CrossRef]

23. Zhong, M.; Xiaorong, C.; Hengyang, M.; Dongqiang, Z.; Shouyong, Z.; Meisheng, L.; Yijiang, Z.; Wenbo, P.; John, H.X. Fabrication of monolithic omniphobic PVDF membranes based on particle stacking structure for robust and efficient membrane distillation. *Desalination* **2024**, *580*, 117547.

24. Chen, L.-H.; Chen, Y.-R.; Huang, A.; Chen, C.-H.; Su, D.-Y.; Hsu, C.-C.; Tsai, F.-Y.; Tung, K.-L. Nanostructure depositions on alumina hollow fiber membranes for enhanced wetting resistance during membrane distillation. *J. Membr. Sci.* **2018**, *564*, 227–236. [CrossRef]

25. Abd Aziz, M.H.; Othman, M.H.D.; Alias, N.H.; Nakayama, T.; Shingaya, Y.; Hashim, N.A.; Kurniawan, T.A.; Matsuura, T.; Rahman, M.A.; Jaafar, J. Enhanced omniphobicity of mullite hollow fiber membrane with organosilane-functionalized TiO₂ micro-flowers and nanorods layer deposition for desalination using direct contact membrane distillation. *J. Membr. Sci.* **2020**, *607*, 118137. [CrossRef]

26. Zou, D.; Lee, Y.M. Design strategy of poly(vinylidene fluoride) membranes for water treatment. *Prog. Polym. Sci.* **2022**, *128*, 101535. [CrossRef]

27. Huang, J.; Chen, C.; Huang, Z.; Fu, J.; Chen, S.; Jiang, Y.; Lu, L.; Xia, Y.; Zhao, X. Preparation and growth mechanism of the flower-like whiskers of γ-, θ-, and α-Al2O3 phases by homogeneous precipitation/calcination method. *Ceram. Int.* **2021**, *47*, 16943–16949. [CrossRef]

28. He, F.; Li, W.; Pang, T.; Zhou, L.; Wang, C.; Liu, H.; Li, M.; He, X. Hydrothermal synthesis of boehmite nanorods from alumina sols. *Ceram. Int.* **2022**, *48*, 18035–18047. [CrossRef]

29. Xu, Q.; Hu, S.; Wang, W.; Wang, Y.; Ju, H.; Zhu, J. Temperature-induced structural evolution of Sm nanoparticles on Al₂O₃ thin film: An *in-situ* investigation using SRPES, XPS and STM. *Appl. Surf. Sci.* **2018**, *432*, 115–120. [CrossRef]

30. Xu, J.; Guan, K.; Luo, P.; He, S.; Matsuyama, H.; Zou, D.; Zhong, Z. Engineering PVDF omniphobic membranes with flower-like micro-nano structures for robust membrane distillation. *Desalination.* **2024**, *578*, 117442. [CrossRef]

31. Li, L.; Wang, J.; Zhong, H.; Hao, L.; Abadikhah, H.; Xu, X.; Chen, C.; Agathopoulos, S. Novel α-Si3N4 planar nanowire superhydrophobic membrane prepared through *in-situ* nitridation of silicon for membrane distillation. *J. Membr. Sci.* **2017**, *543*, 98–105. [CrossRef]
32. Boffa, V.; Lunghi, C.; Quist-Jensen, C.A.; Magnacca, G.; Calza, P. Fabrication and Surface Interactions of Super-Hydrophobic Silicon Carbide for Membrane Distillation. *Nanomaterials* **2019**, *9*, 1159. [CrossRef]